HAL
open science

Basal slip localization in zinc single crystals. The Considére analyses

Miroslaw Wróbel, Krzysztof Piela

To cite this version:

Miroslaw Wróbel, Krzysztof Piela. Basal slip localization in zinc single crystals. The Considére analyses. Philosophical Magazine, 2010, 90 (14), pp.1873-1891. 10.1080/14786430903571446 . hal-00587605

HAL Id: hal-00587605

https://hal.science/hal-00587605v1

Submitted on 21 Apr 2011

HAL is a multi-disciplinary open access archive for the deposit and dissemination of scientific research documents, whether they are published or not. The documents may come from teaching and research institutions in France or abroad, or from public or private research centers.

L'archive ouverte pluridisciplinaire **HAL**, est destinée au dépôt et à la diffusion de documents scientifiques de niveau recherche, publiés ou non, émanant des établissements d'enseignement et de recherche français ou étrangers, des laboratoires publics ou privés.

Basal slip localization in zinc single crystals. The Considére analyses

Journal:	*Philosophical Magazine & Philosophical Magazine Letters*
Manuscript ID:	TPHM-09-Jun-0280.R1
Journal Selection:	Philosophical Magazine
Date Submitted by the Author:	23-Oct-2009
Complete List of Authors:	Wróbel, Mirosław; AGH University of Science and Technology, Metal Engeenering and Industrial Computer Science Piała, Krzysztof; AGH University of Science and technology, Non-Ferrous Metals
Keywords:	crystals, deformation, mechanical testing, strain, stresses, tensile, compression
Keywords (user supplied):	strain localization, necking, zinc

scholarONE™
Manuscript Central

Basal slip localization in zinc single crystals. The ConsidΠre analyses

M. Wróbel, K. Pieła

AGH University of Science and Technology
30 Av. Mickiewicza, Pl. 30-059 Kraków, Poland

Corresponding Author: M. Wróbel, AGH University of Science and Technology, 30 Av. Mickiewicza, Pl. 30-059 Kraków, Poland, tel. 4812 617 3867 fax. 4812 617 3344, e-mail: mwrobel@agh.edu.pl

Key words: zinc, single crystals, strain localization, necking, tension, compression

Summary

The tensile and compression tests of zinc single crystals oriented for slip in the basal slip system were performed. During the first stage of the stress-strain curve, the localized necking was typical to the strain localization in the tensile specimens. Single or multiple necks were formed along the specimen length. The range of temperature and the strain rate for the single necking of the sample was determined. It was found that the formation of such necking depends on strain hardening characteristics and can be predicted by the ConsidΠre criterion. On the other hand, propagation of the necked area along the sample length was not predictable by this criterion.

Localized sliding and specimen kinking was indicative of the strain localization observed for different specimens compressed under the same conditions, i.e., temperature and strain rate. A decrease in the compression force and in the cross-sectional area with anvils displacements produced localized sliding. On the other hand, a continuous increase in the compression force was representative of tests leading to specimen kinking.

1. Introduction

Early tensile tests conducted on the zinc single crystals oriented for slip in one basal slip system (soft oriented crystals) show that their mechanical characteristics as well as macrostructures essentially depend on the test temperature. The typical three-stage curve of the shear stress τ vs. shear stain γ (labeled as A, B and C, respectively, Fig. 1) was registered only for a narrow range of test temperatures (i.e., 0.40-0.55 T_m where T_m – the melting point), and it is replaced by a two-stage (A and B) curve at the test temperature close to 0.7 T_m. This change is accompanied by a rapid decrease in the work-hardening rate at stages A and B (to values close to zero) and the increase in the range of easy glide (A) [1-7]. The higher test temperature (above 0.7 Tm) leads to a decrease in plasticity and an increase in the value of the 'mean' work-hardening coefficient of zinc crystals [8, 9]. Pieła [10-12] showed that the temperature anomalies are closely connected with the processes of macroscopic localization of slip in the basal system, especially with the transition from single necking to crystal 'fragmentation' caused by multinecking with kink bands formation. Moreover, it was shown that the tendency toward the basal slip localization was not confined to the tensile specimens. Specimen kinking in a single broad region or in several narrow areas was typical to strain localization in the compressed zinc crystals [11, 12].

For Peer Review Only

The present work investigates in detail these strain inhomogeneities during the initial stage (A) of the $\tau(\gamma)$ curve of zinc crystals for which deformation proceeds only in the basal slip system. The influence of deformation rate and temperature as well as the ratio of the gauge length to the sample diameter (aspect ratio) on the form of strain localization was investigated. The applicability of the ConsidΠre criterion [13, 14] for such strain localization was tested. Verification of the applicability of that criterion for strong strain localization, such as necking, which occurred in zinc single crystal in the regime of single glide deformation, is important since some experimental results have lead to the conclusion that "ConsidΠre criterion is almost never exhibited by single crystals deformed in tension and not always by polycrystalline specimens" [15].

2. Experimental

The experiment was carried out on cylindrical (Ø6 mm) zinc single crystals of 99.995% purity, obtained by the Bridgman method (with the vertical gradient of the temperature). Crystals were deformed in tension or compression at constant temperature and strain rate on Instron 1115 and Instron 6025 test machines. Before deformation, each sample was carefully etched in an HCl solution in water and then chemically polished in HNO_3 solution in water.

Crystals of two initial orientations, i.e., $\lambda_o = 52^o$, $\chi_o = 38^o$ and $\lambda_o = 45^o$, $\chi_o = 45^o$ (where: λ_o, χ_o, - angle between the crystal axis and the normal to the basal plane of slip (0001) and the slip direction $\langle 1\ 1\ \bar{2}\ 0\rangle$, respectively) were used in tensile testing and labeled correspondingly as I and II (table 1). The ends of the tensile samples were affixed into steel rings with a zinc mold and then inserted into the grips of the tensile machine.

The initial gauge length of the tensile single crystals with orientation I was 20 mm and with orientation II was in the range of 15 - 60 mm; the aspect ratios of the samples in the two orientations were 3.3 and 2.5 – 10, respectively. Tensile tests of crystals with orientation I covered the range of temperatures from 373 K to 673 K and strain rates from $8x10^{-4}$ to $8x10^{-2}$ s^{-1}. The strain rate for the tensile tests of crystals with orientation II was equal to $8x10^{-3}$ s^{-1}, and the tensile temperatures ranged from 373 K to 573 K.

Cylindrical single crystals (Ø6 mm) with orientation $\chi_o = 30^o$, $\lambda_o = 61^o$ (labeled as III) and initial length equal to 12 mm were compressed in a wide range of temperatures, 293-673 K, and strain rates from $1.3x10^{-5}$ to $8x10^{-3}$ s^{-1}. Friction between the specimens and anvils were reduced by a graphite lubricant covering the loaded ends of the specimen.

For tensile and compression tests, the total elongation divided by the initial gauge length and the elongation rate divided by the initial gauge length were used as a deformation measure and a deformation rate measure, respectively.

Slip lines produced during deformation on the polished specimens surfaces were examined by optical microscopy.

For selected specimens deformed by tension, the 0002 X-ray pole figures were measured by the use of the Cu Kα radiation on the Brucker D8 Discover goniometer. The diameter of discs from which the pole figures were measured was ca. 1 mm. Two sets of measurements were taken. For the first set, the X-ray intensities were registered for an angular position of the sample from a range of $\alpha = 0 - 80^o$, $\Delta\alpha = 5^o$ and rotation around normal direction (ND), $\beta = 0 - 360^o$, $\Delta\beta = 5^o$. Measurements were performed in three points located in the necked zone, far from the neck, and also from the zone in which the neck was formed. For the other set of measurements the orientation changes were mapped in 43 points distributed along the tensile axis on the entire length of the zone were the neck was formed. The distance between the neighboring points was equal to 0.5 mm. For these measurements

For Peer Review Only

the X-ray intensities were registered for the angular position of the sample α = 0 - 50°, $\Delta\alpha$ = 1°, β = -5 - 20°, $\Delta\beta$ = 1°, Fig. 6b.

In the selected regions located along the gauge length of the tensile deformed single crystal the crystallographic orientations were measured by the use of the electron backscatter diffraction (EBSD) on a scanning electron microscope (SEM). The microscope used was the Philips XL-30 SEM equipped with the NORDIF EBSD hardware and the CHANNEL-HKL EBSD software for registration and fully automated indexing of the electron backscatter diffraction (EBSD) patterns.

3. Results and discussion

3.1 Tensile tests

The typical force–elongation curves are shown in Figs. 2, 3. Depending on the tensile test conditions, crystals with orientation I could be deformed up to 200-1000% (Fig. 4a). The deformation obtained in the stage A of the stress-strain curve lay between 20% to 80% of total deformation (Fig. 4b, c). Similarly, large deformations in the stage A were observed for crystals in orientation II, so both selected crystallographic orientations ensured a relatively high range of deformation occurring primarily by slip in the basal plane. This observation was confirmed by observation of the slip line pattern formed on the specimens' surfaces (Fig. 5). As was verified by selected specimens, rotation of the orientation determined from X-ray pole figures and from EBSD- patterns was the same as the rotation expected for the slip in the basal plane (Fig. 6, 7). A very low strain hardening observed on the tensile curves is also typical for the slip on a single slip plane, Fig. 3.

The plastic deformation was initiated in one or more areas along the gauge length, and was initially confined to these regions. As such, single or multiple necks formed along the sample length. Single necking was expected for crystals with orientation I due to their relatively short length (i.e., 20 mm). However, it was found that single necking was observed for both crystal orientations and for crystals with significantly different lengths. Single necking corresponded to samples showing the highest elongation and the highest amount of strain in the first stage of the stress-strain curve (the A-stage of the plastic deformation). The test conditions (temperatures and strain rates) for such samples in orientation I are shown in Fig. 8. The increase in the strain rate from $8x10^{-4}$ s^{-1} to $8x10^{-2}$ s^{-1} shifted the temperature range of single necking from approx. 473-523 K to approx. 548-573 K. For the higher temperatures, multinecking was usually observed. It was found that there is a greater tendency toward multinecking when the strain rate decreases. This can be correlated to the increased tendency for the initiation of plastic deformation induced by local heterogeneities of the stress field occurring with decreasing strain rate. Such heterogeneity acts as a local stress concentrator. The local stress concentrations can result from imperfections in the sample surface (for example due to the surface roughness) and/or from some reasons related to microstructure (for example heterogeneity in the dislocation distribution).

Effect of the aspect ratio on the strain distribution along the gauge length of the sample is shown in Fig. 9 for crystals with orientation II. For all crystals shown in the figure, the average deformation was 100%, and the deformation rate was equal to $8x10^{-3}$ s^{-1}. Single necking and the maximum local deformation were registered for the test temperature 523 K. For the higher test temperatures, the occurrence of multinecking was a typical behavior, especially for longer crystals. Susceptibility of the longer specimens to multinecking can be related to the increase in probability of a local stress heterogeneity which increases with the gauge length of the specimen.

The deformation was initially localized in the neck region, and local reduction in the cross section area of the sample increased with deformation. About 90% of deformation was

For Peer Review Only

localized in the neck region where the maximum reduction in the cross section area occurred. However, after some further reduction in area the basal slip plane was slightly inclined to the tensile axis and the neck deepening stopped. Continuation of the neck deepening would require an additional slip in a non-basal plane, but critical stresses for such slip are much higher then that for basal plane slip. The deformed region propagated along the gauge length of the sample until the neck ultimately vanished. The average value of the maximum reduction in cross section in the neck were equal to 52±17% and 73±8% respectively for orientations I and II; therefore, the tendency for localization of the deformation in the neck was higher for orientation II. The prominent value of local deformation resulted in stresses significantly higher than those in regions with little or no plastic deformation. For example, for one of the specimens with an average deformation of 80%, the tensile stress inside of the long neck was approximately four times larger than that acting in the region in which the neck propagated. This indicates that, due to low strain hardening, the propagation stresses are much higher than the stresses required for localization of the deformation.

Stresses acting in the area of the very deep neck are high and they could be sufficient for activation of the non-basal plane slip during high temperature deformation. Such a change in active slip systems should influence texture and microstructure. The shift of rotation axis of the texture maximum, like that shown in Fig. 6b, might have been related to the activation of the non-basal plane slip, but an occurrence of this type slip was not revealed in the microstructure (Fig. 5). However, for some specimens deformed at high temperature non-basal plane slip cannot be excluded, so verification of the non-basal plane slip required further investigation. No increase in the deepness of the propagating neck, as was observed in our experiment, suggested that, even if the non-basal slip was activated, its amount was rather small. Nevertheless, the doubtful data were not used for analyses presented in the next chapter of our work.

3.2. Theoretical analyses of the strain localization

An understanding of the stress state is necessary for analyses of the strain localization from a mechanical point of view. Since a simple uniaxial stress can be related to the tensile test, our analyses were limited to the tensile specimens.

ConsidΠre first published the criterion for the necking of tensile rods [13]. According to his criterion, necking of a polycrystalline specimen, insensitive to deformation rate, requires that the following condition is satisfied:

$$dP/d\varepsilon<0, \quad (1)$$

or alternatively

$$d\sigma/ d\varepsilon < \sigma, \quad (1a)$$

where: P- tensile load, ε- true strain, σ- true flow stress. Stηwe and Toth [14] formulated the ConsidΠre criterion using the resolved shear strain γ_r, the critical resolved shear stress τ_{rc} and the Taylor factor $M = \dot{\gamma}_r / \dot{\varepsilon}$ (which is the reciprocal of the Schmid factor for the single crystals oriented for single slip):

$$H = (1/\tau_{rc}) *(d\tau_{rc}/d\gamma_r) < S = (1/M)*(1-(dM/d\gamma_r)). \quad (2)$$

The left hand side of the inequality (2) defines the intristic hardening (H). The right hand side of the inequality describes the geometric effects (the cross section reduction and the orientation factor changes) and defines the instability factor (S) depending on the

For Peer Review Only

crystallographic structure and orientation. For single crystals oriented for single slip, the value of S can be calculated from the following equation [14]:

$$S = \cos\chi\,(\frac{1}{\cos\lambda} - \cos\lambda) = \frac{e^{-3\varepsilon}\cos\chi_o \sin^2\lambda_o}{\sqrt{1-e^{-2\varepsilon}\sin^2\lambda_o}}\ , \qquad (3)$$

where: χ- the angle between the slip direction and the loading axis, λ- the angle between the slip plane normal and the loading axes, both for the orientation after deformation ε, χ_o and λ_o that same angles but for the initial orientation.

In the ConsidΠre criterion the strain rate effect was neglected. Such effects should be considered for metals exhibiting significant strain rate sensitivity (as zinc), so criterion (2) should be supplemented by additional terms. Unfortunately, the data obtained in the present work were not sufficient for such analyses, so the strain rate effects were also neglected. As a consequence, we used inequalities (1, 2) derived under the additional assumption that the resolved shear stress in the activated slip system τ_r is equal to the critical shear stress τ_{rc} (the internal and external states of stress were in equilibrium, hence forward referred as the stress equilibrium condition).

The ConsidΠre criterion (inequality (1a)) is always fulfilled for a negative hardening rate ($d\sigma/d\varepsilon<0$). For the positive hardening rate, the ConsidΠre criterion is used to predict the length of the macroscopically homogenous range of the plastic deformation. The ConsidΠre criterion (inequality (1)) can also predict the strain localization in the form of Lηders-band for a drop in the specimen load. In the present work, we decided to check if the criterion in the form proposed by Stηwe and Toth (inequality (2)) can predict the susceptibility for pronounced necking as was observed during single slip deformation of zinc crystals.

For orientations II and I the initial value of S was equal to 0.5 and 0.296, respectively. The effect of the resolved shear strain γ_r in the basal system for the single slip deformation on the instability factor for both orientations is shown in Fig. 10. Differences in S decreased with increasing γ_r, but up to a high value of shear the deformed crystals with initial orientation II had significantly higher S than those with initial orientation I. This indicates that the susceptibility to localization of strain is higher for orientation I rather than for orientation II. On the other hand, a higher maximum deformation in the neck was observed for deformed crystals with initial orientation II; therefore, as expected, the value of S is not related to deformation in the region of localized deformation (neck). Instead, the maximum deformation in the neck is determined by the crystallographic orientation that limits the maximum angle of the lattice rotation during deformation. Such rotation leads the slip direction into a position parallel to the tensile axis and the rotation angle can be higher for orientation II.

For the investigated crystals, the experimental determination of the function $H(\gamma_r)$ was difficult because necking started at the very beginning of plastic deformation and the neck developed with further deformation. Generally, the function cannot be calculated directly from the tensile curve because of the tri-axial state of stress developed in the neck areas. Calculation of $H(\gamma_r)$ under the assumption of uniaxial stresses is possible but can only be considered as a rough approximation. Generally, this assumption is only fulfilled for the deformation preceding necking. However, it was quite well fulfilled at the onset of necking within the areas far from the ends of relatively long, diffused necks like that observed in the crystal deformed at 523 K (Fig. 9a). This assumption significantly reduces the amount of data useful for analyses. Assuming uniaxial stresses, the resolved shear stress τ_r can be calculated from the equation:

For Peer Review Only

$$\tau_r = (P/A_0)*\cos\lambda_0\sqrt{1-(e^{-2\varepsilon}\sin^2\chi_0)} = (P/A_0)*\cos\lambda_0\sqrt{(1-\frac{\sin^2\chi_0}{(\gamma_r*\cos\lambda_0+\cos\chi_0)^2+\sin^2\chi_0}}\,, \qquad (4)$$

where A_0 – the cross-sectional areas of the undeformed crystal.

For the assumed infinitely low rate of the deformation (stress equilibrium condition), τ_r from equation (4) is equal to τ_{rc} and could be directly used for the calculation of $H(\gamma_r)$ according to the left hand side of the inequality in (2). $H(\gamma_r)$ functions were calculated for the selected relationship between the force P and extension. The force decreased with the sample extension for the initial stage of deformation when the neck was formed and then increased in the depth, as is shown in Fig. 11a. As an example the decrease in force with deformation in the initial range of the tensile curve (A1) from Fig. 11a, can be approximated by the equation: $P = 0.0197 - 0.0002*\varepsilon + 4*10^{-6}*\varepsilon^2$, where P is in kN and ε, the sample extension, is expressed in %. Fig 11b shows that for a decreasing force, $H(\gamma_r) < S(\gamma_r)$, so the inequality (2) is fulfilled and necking is predicted by the ConsidΠre criterion. The necking condition is satisfied from zero strain so the neck was formed and increased in depth.

For the second stage of deformation (A2 in Fig. 11a), the force was nearly constant or increased with the specimen elongation depending on the test condition. Based on the experimental results, calculations for the second deformation range were performed with the assumption of the deformation under a constant tensile force equal to $2.32\text{x}10^{-2}$ kN (i) and the P increased with ε and is approximated as: $P = 1.19\text{x}10^{-2} + 2\text{x}10^{-4}\,\varepsilon$ (ii) and as $P = 1.98\text{x}10^{-2} - 2\text{x}10^{-4}\,\varepsilon + 3\text{x}10^{-6}\,\varepsilon^2$ (iii). The actual increase in force is considerably smaller, and the above equation can be treated as an upper bound. Fig. 12 shows that in this case $H(\gamma_r) > S(\gamma_r)$. The inequality in (2) is no longer fulfilled, so according to the ConsidΠre criterion any new neck could not be formed. As was observed, the neck propagated along the gauge length and the depth of this propagated neck was not changed.

It should be mentioned that for the ConsidΠre analysis, the stress equilibrium condition was assumed. From the Schmid law, the specimen locally deforms under the condition that $\tau_r = \tau_{rc}$. The small strain hardening effect of zinc facilitates the deformation localization. However, as τ_{rc} increases due to strain hardening such that $\tau_r < \tau_{rc}$, the deformation must be transferred to other volume elements of the specimen where the Schmid law is satisfied. Depending on the local value of τ_{rc} and the local stress concentrators, this can be realized by either neck propagation or by necking in another place of the specimen. Thus, the initial localization of the plastic deformation in a single slip system in the form of necking propagating along the specimen with proceeding deformation can be more akin to the Lηders type localization of plastic deformation than the typical necking observed during the last stages of tensile tests. The deformation therefore was confined primarily to the area where the neck was formed or were it propagated. In areas of the diffused necks, patterns of the slip lines indicated that the necking was not in the form of kinking and was more diffuse than slip banding, Fig. 5. Our observation confirmed that the difference in the strain along the necked crystals can be accommodated by some bending of the sample, as was predicted by Gilman [16]. Kinking (the second form of such accommodation) was observed in some crystals, particularly with low aspect ratio and/or multinecked, Fig. 13. A similar situation concerning compression and some form of the strain localization can be expected in compression tested single crystals. A detailed microscopic description of such a heterogeneous deformation is very complicated, since it requires knowledge of stress, strain and strain rate distribution on the length of deformed specimen. However, such an approach is beyond the scope of the

For Peer Review Only

present work. What is more, the ConsidΠre criterion is not applicable for compression tests for which the area of the compressed cross-section increases.

3.3 Compression tests

Almost all crystals compressed at 293 K and some of those compressed at 373 K and at the temperatures from 573 K to 673 K sheared more or less homogenously or barreled (Fig. 14). The changes in the shape of specimens during compression resulted not only from the eventual tendency to strain localization, but also depended on the constraints at the loaded ends, due to friction between the specimen and anvils. For deformation in one slip plane, the homogenous shearing of the specimen demonstrated frictionless conditions at the loaded ends of the specimen. In such a case, the test can be approximated as unidirectional compression. On the other hand, barreling of the specimens indicated pronounced friction that induced a complicated combined state of stress in the compressed specimen.

Some effects of the strain localization was observed for the specimens deformed at temperatures from 373 K and 423 K to 573 K and 523 K, respectively for the strain rates $8x10^{-5}$ s^{-1} and $8x10^{-3}s^{-1}$. The strain localization manifested in one of two ways: as specimens kinking or as localized sliding of the specimen. Both of them indicated nearly frictionless conditions at the loaded ends of the specimens and differed in the extent of local deformation and volume of highly deformed material. For specimen kinking, the average local deformation was lower but the deformed volume was so large that the specimen bent, as representatively shown in Fig. 14a for the specimen compressed at 373 K. On the other hand, the localized sliding was limited usually to one, two or three relatively narrow and much more highly deformed areas of the specimen. Such areas were separated by effectively undeformed material, and steps were formed on the specimen (Fig. 14). Sometimes both manifestation of strain localization were formed on the same specimen. A hybrid of strain localization effects with almost homogenous shearing or barreling of the sample was also observed, but only for deformation conditions from the boundary of the region limiting observation of strain localization.

We observed the specimen kinking as the typical form of the strain localization. According to our knowledge, the term 'specimen kinking' was introduced into the literature by Orowan [17] who observed it in compressed cadmium single crystals. Earlier kinking was observed in a variety of mineral crystals [18, 19] and later confirmed for metals with hcp or B2 structure (i.e., Zn and NiAl) [19-21]. On the other hand, the localized sliding (also referred to as the catastrophic flow) was observed in crystals with fcc [23] and bcc [24-28] structures. Formation of both types of the microstructure inhomogeneities in compressed zinc was reported in Ref. [12].

Specimen kinking is a type of reaction that compensates for the non-coaxial position of loaded faces due to their displacements by a high deformation in one slip plane, concentrated in the central part of the specimen. An increase in the compression force with anvil displacement was registered for this type of deformation. The similar character of the force-displacement curve was typical for tests producing nearly homogenously sheared or barreled specimens. On the other hand a decrease in the compression force with anvil displacements was typical for tests producing localized sliding and for the hybrid of them with almost homogenous shearing of the specimen, Fig. 15. The localized sliding could fulfill conditions of the ConsidΠre criterion because of the decrease in the compression force and in the local specimen cross-section area with anvil displacements. Verification of the criterion validity requires additional experiments. The deformation conditions such as that during localized sliding were not fulfilled for the tests producing kinked, nearly homogenously sheared or barreled specimens. All such forms of deformation were observed in different samples compressed under the same conditions. Therefore, it is very likely that localized sliding can

For Peer Review Only

be similarly explained as necks formed during the first stage of the stress-strain curve (section 3.2).

The localized sliding was promoted by the test conditions. It was observed only for some specimens deformed in a narrow range of temperatures and was favored by a lowering of the deformation rate. For the deformation rate of $1.3x10^{-5}s^{-1}$ it was realized in the temperatures from 423 K up to 573 K. The increase in the deformation rate to $8x10^{-5}s^{-1}$ and to $8x10^{-3}s^{-1}$ narrowed the temperature range to 473-548K and 523-548 K, respectively. Other samples, deformed under the same conditions, kinked. Also Chan et al. [27] observed the localized sliding for some single crystals of Nb and believed that such a heterogeneity was not the typical form of the strain distribution over the sample volume. The above results demonstrate the sensitivity of the localized sliding to some imperfections of the tests or inhomogeneities in the sample macro- or microstructure. The decrease in tendency for sliding observed in our experiment for the higher deformation rates suggests a correlation to sample perfection rather than to errors of the deformation test itself. As was observed by Pieła [12], the tendency for the localized sliding increases with perfection of the substructure (a smaller mosaic) formed during growth of the single crystals. On the other hand, it cannot be excluded that the type of localization results from the differences in distributions of the deformation seeds within the samples, e.g. due to even fine differences in the surface roughness of the examined specimens.

4. Conclusions

1. During the easy glide stage of the zinc single crystals deformation, the neck was formed and initially increased in the depth. After some amount of deformation the neck deepening stopped, and the deformation proceeded by propagation of the neck along the sample length.

2. Formation of the neck can be predicted by the ConsidΠre criterion. On the other hand, the propagation of the necked area along of the gauge length during the first (easy glide) stage of the deformation is not described by this criterion.

3. The form of the ConsidΠre criterion, proposed by Stηwe and Toth [14], can be useful to predict the susceptibility of different crystallographic orientation for strain localization

4. Single necking was observed for the specimens deformed in tension in the range of temperatures approx. 473-523 K and the strain rate $8x10^{-4}$ s^{-1} and was shifted to temperatures approx. 548-573 K when the strain rate increased to $8x10^{-2}$ s^{-1}. A multinecking state was typical behavior for the higher temperatures, especially for the lower strain rates.

5. Localized sliding and specimen kinking were characteristic forms of strain localization for the compressed specimens. Both forms of the strain localization were revealed in specimens compressed in the temperatures from 423 K up to 573 K with the strain rate of $1.3x10^{-5}s^{-1}$. The increase in the strain rate to $8x10^{-5}s^{-1}$ and to $8x10^{-3}s^{-1}$ confined that range of temperatures to 473-548 K and 523-548 K, respectively.

6. The decrease in the compression force and in the cross-sectional area of the deformed sample with anvil displacements was distinctive for tests producing localized sliding. The increase in compression force with anvil displacement was observed for tests producing specimen kinking and for specimens nearly homogenously sheared or barreled.

For Peer Review Only

Acknowledgements
The financial support of AGH, contracts no 11.11.180.792 and 11.11.180.448, is appreciated. We thank Prof. J. Bonarski from A. Krupkowski Institute of Polish Academy of Sciences for his help during X-ray measurements.

References

1. M. Boček, G. Hötzsch, Phys. Stat. Sol. 6 (1964) p. 777.
2. M. Boček, G. Hötzsch, Phys. Stat. Sol. 7 (1964) p. 373 .
3. M. Boček, G. Hötzsch, B. Simmen, Phys. Stat. Sol. 7 (1964) p. 833.
4. M. Boček, V. Kaśka, Phys. Stat. Sol. 4 (1964) p. 325.
5. M. Boček, P. Lukáč, B. Smola, M. Švábová, Phys. Stat. Sol. 7 (1964) p. 173.
6. K. Lücke, G. Masing, K. Schröder, Z. Metallkunde 46 (1955) p. 792.
7. A. Seeger, H. Träuble, Z. Metallkunde 51 (1960) p. 435.
8. E. Schmid, W. Boas, *Kristallplastizität*, ed. Springer Verlag, 93, Berlin 1936
9. O. A. Kajbyshev, W. W. Astatin, R. Z. Valijew, FMM 46 (1978) p. 1297.
10. K. Pieła, Arch. Metall. 36 (1991) p. 311.
11. K. Pieła, Arch. Metall. Mater. 49 (2004) p. 705.
12. K. Pieła, Rozprawy i monografie, z. 133, AGH, Kraków, 2004 /in polish
13. A. ConsidΠre, Ann. des Ponts et Chaussees 9 (1885) p. 574.
14. H. P. Stüwe, L. S. Toth: Mat. Sci. Eng. A358 (2003) p. 17.
15. Z.S Basinski, M. S. Szczerba, J.D. Embury, Phil. Mag. 76 (1997) p. 743.
16. J. Gilman, Trans. Met. Soc. AIME, 200 (1954) 621
17. E. Orowan, Nature 149 (1942) p. 634.
18. O. Mηgge, Neues. Jahr. f.Miner., 7 (1898) 71
19. J.B. Hess and C.S. Barret, Met. Trans. 185 (1949) p. 599.
20. R.T. Pascoe, C.W.A.Newey, Phys. Stat. Solid. 29 (1968) p. 357.
21. R.T. Pascoe, C.W.A.Newey, Met. Sci. J. 2 (1968) p. 138.
22. H.L. Fraser, R.E. Smallman and M.H. Loretto, Phil. Mag. 28 (1973) p. 651, p. 657.
23. A.H. Cottrell, *The mechanical properties of materials*, J. Wiley & Sons, Inc., New York, 1940, Warszawa, 1970, p. 400
24. E. Votava, Phys. Stat. Sol. 5 (1964) p. 421.
25. C.N. Reid, A. Gilbert, G.T. Hahn, Acta Met. 14 (1966) p. 975.
26. L. P. Kubin, B. Jouffrey, Phil.Mag. 24 (1971) p. 437.
27. C.Y. Chan, C.N. Reid, B.J. Duggan, Mat. Sci. Techn. 18 (2002) p. 449.
28. B. Dubiel, M. Wróbel, P.J. Ennis, A. Czyrska-Filemonowicz, Scripta Mat. 37 (1997) p. 1215.

For Peer Review Only

Table 1. Details of mechanical tests

Orientation λ_o /χ_o (designation)	Gauge length and the aspect ratio (in brackets) of the sample	Deformation tension / compression	Test temperature and strain rate
52° / 38° (I)	20 (3.3)	+ / -	373 - 673 K/8*10^{-4}-8*10^{-2} s^{-1}
45° / 45° (II)	15-60 (2.5-10)	+ / -	373 - 573 K/8*10^{-3} s^{-1}
30° / 61° (III)	12 (2)	- / +	293 - 673 K/1.3*10^{-5}-8*10^{-3} s^{-1}

For Peer Review Only

List of Figures

Fig. 1
Typical three-stage shear stress vs. shear strain curve for tensile deformed single crystals with the soft initial orientation.

Fig. 2
Force vs. elongation curves for tensile deformed single crystals with orientation I.

Fig. 3
Effect of the test temperature on first stage of the elongation curves, orientation I, strain rate $8*10^{-3}s^{-1}$

Fig. 4
Influence of the tensile condition on the elongation of the crystals with orientation I, (a) the total elongation (ε), (b) share of the elongation in the stage A of the stress-strain curve in the total elongation ($\varepsilon_A/\varepsilon$), (c) the elongation in the stage A of the stress-strain curve.

Fig. 5
Slip line pattern produced during tension on the crystal surface; region of the neck, optical microscopy, (a) bright field images, (b) image obtained by use of the Nomarski Interference Contrast; orientation II, temperature 473 K, strain rate $8*10^{-3}s^{-1}$, elongation 50%

Fig. 6
0002 X-ray pole figures determined on the ED-TD cross section in different points on gauge length of the tensile single crystal, orientation I, (a) registered for angular position of the sample covered inclination $\alpha = 0 - 80^o$, $\Delta\alpha = 5^o$ and rotation around ND, $\beta = 0 - 360^o$, $\Delta\beta = 5^o$, (b) position of the 0002 maximum for points no. 1-43, registered for $\alpha = 0 - 50^o$, $\Delta\alpha = 1^o$, $\beta = -5 - 20^o$, $\Delta\beta = 1^o$; orientation II, temperature 523 K, strain rate $8*10^{-3}s^{-1}$; ED-elongation direction, ND- normal direction, TD-transverse direction. Notice a shift of rotation axis of the texture maximum (points 1-14 and 15-43).

Fig. 7
The results of EBSD-measurements in two regions (A and B) on the ND-ED cross-section of the tensile single crystal, orientation and the deformation conditions that same as for crystal from Fig. 6; (a) 0002-pole figure, (b) the line scan of the misorientation along ED; misorientations determined with respect to the first point of measurement (on the left side of the figures (b) and (d)), (c) typical line scan of the misorientation along ED; misorientations determined for neighboring points of measurement, (d) schematic position of investigated regions. Notice rotation of the orientation in region A and a small misorientation for the neighboring points.

Fig. 8.
Effect of the deformation condition on macrostructures of zinc single crystals with orientation I deformed to 100%; strain rate: (a) 8×10^{-4} s^{-1}, (b) 8×10^{-2} s^{-1}.

For Peer Review Only

Fig. 9.
Effect of the sample geometry (the length to diameter ratio) on macrostructures of zinc single crystals with orientation II elongated to 100%. Ratio length to diameter of crystals: (a) 10, (b) 2.5; strain rate 8 x 10^{-3} s^{-1}.

Fig. 10
Changes in the instability factor S with the strain in the basal system γ_r for the single slip of crystals with initial orientation I and II.

Fig. 11
Typical force (P) – elongation (ε) relationship, initial orientation II, temperature 473 K, strain rate 8x10^{-4} s^{-1} (a) and the corresponding changes in the factor of instability $S(\gamma_r)$ and in value of the intristic hardening parameter $H(\gamma_r)$ with the resolved shear strain in the basal slip system γ_r (b). $H(\gamma_r)$ was calculated for the decreased range of the force-elongation curve (A1) which up to approx. $\gamma_r = 0.46$ ($\varepsilon < 25\%$) can be approximated by equation: $P = 1.97\text{x } 10^{-2} - 2\text{x}10^{-4}\varepsilon + 4\text{x}10^{-6}*\varepsilon^2$, $R^2 = 0.99$, where P is in kN and ε the sample elongation, expressed in %. Relation between γ_r and ε can be expressed as: $\gamma_r = (1/\cos\lambda_0)(\sqrt{(1+0.01\varepsilon)^2 - \sin^2\chi_0}) - \cos\chi_0)$

Fig. 12
Changes in the factor of instability $S(\gamma_r)$ and in the intristic hardening of the material $H(\gamma_r)$ with the resolved shear strain in the basal slip system γ_r for crystal with initial orientation II. $H(\gamma_r)$ was calculated for selected experimentally determined relationship of the tensile force (P, in kN) vs. elongation (ε in %) observed for A2 deformation stage (after initial decrease in the tensile force).

Fig. 13
Slip line pattern produced during tension on the crystal surface; region of the typical kink band; orientation II, temperature 573 K, strain rate 8*$10^{-3}s^{-1}$, elongation 10%.

Fig. 14.
Macrostructures of compressed zinc single crystals. Orientation III; strain rate: (a) 8x10^{-5} s^{-1}, (b) 8x$10^{-3}s^{-1}$.

Fig. 15
Typical compression curves with corresponding macrostructures, orientation III, strain rate 8*$10^{-5}s^{-1}$ for temperatures 473 K and 523 K and 1.3 *$10^{-5}s^{-1}$ for 423 K and 573 K. Notice that the localized sliding corresponds to a decrease in the compression force and in the local specimen cross-section area with anvil displacements.

For Peer Review Only

Basal slip localization in zinc single crystals. The ConsidΠre analyses

M. Wróbel, K. Pieła

AGH University of Science and Technology
30 Av. Mickiewicza, Pl. 30-059 Kraków, Poland

Corresponding Author: M. Wróbel, AGH University of Science and Technology, 30 Av. Mickiewicza, Pl. 30-059 Kraków, Poland, tel. 4812 617 3867 fax. 4812 617 3344, e-mail: mwrobel@agh.edu.pl

Key words: zinc, single crystals, strain localization, necking, tension, compression

5927 words

For Peer Review Only

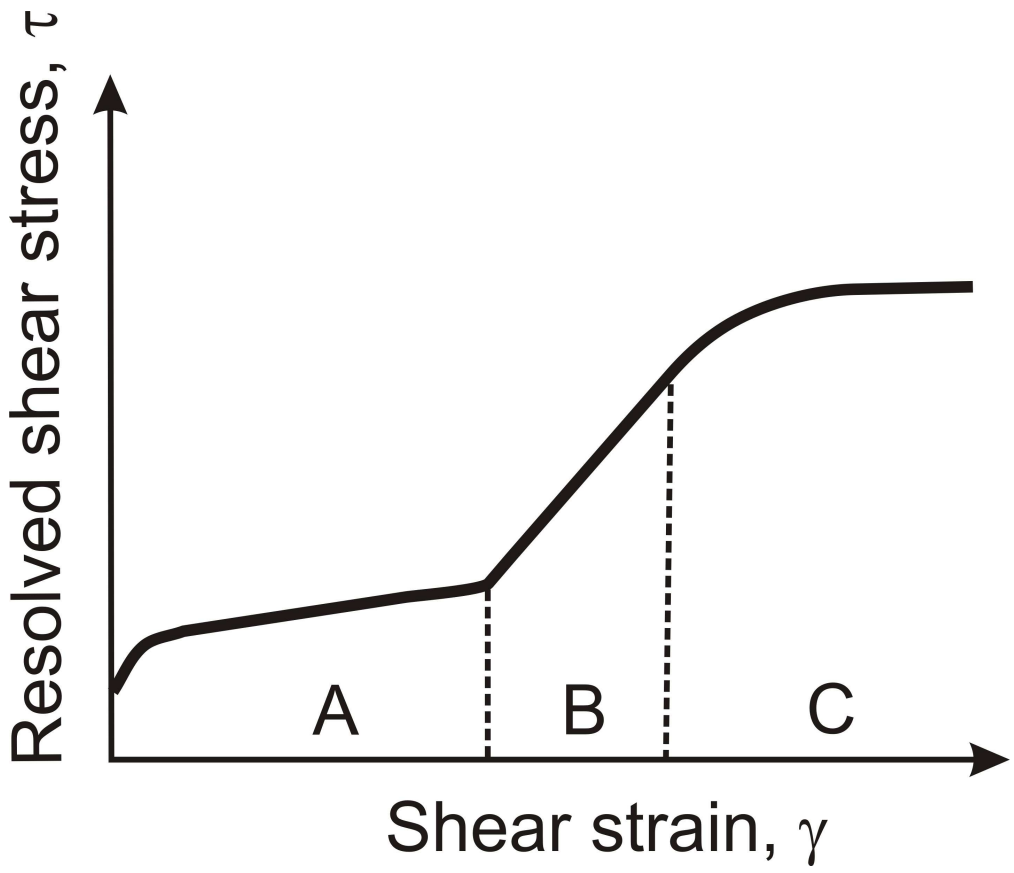

121x103mm (600 x 600 DPI)

w Only

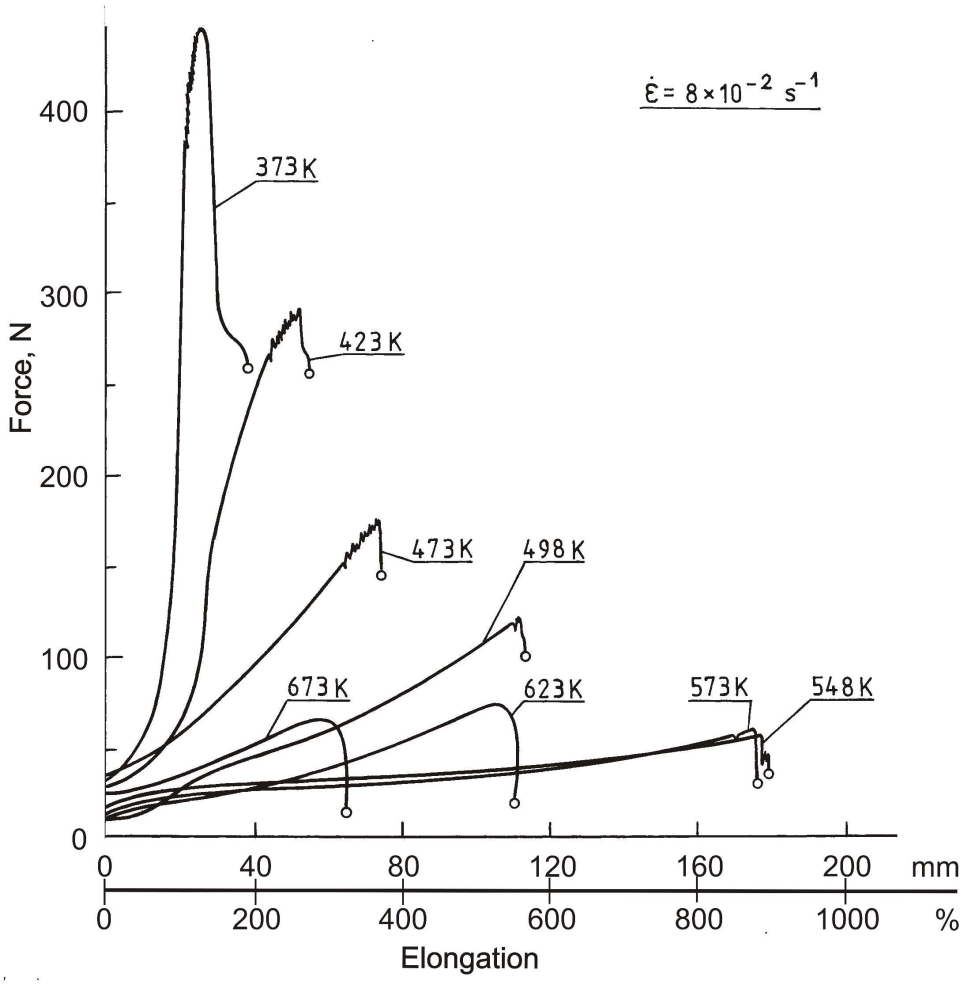

192x193mm (600 x 600 DPI)

Unable to Convert Image

The dimensions of this image (in pixels) are too large to be converted. For this image to convert, the total number of pixels (height x width) must be less than 40,000,000 (40 megapixels).

Peer Review Only

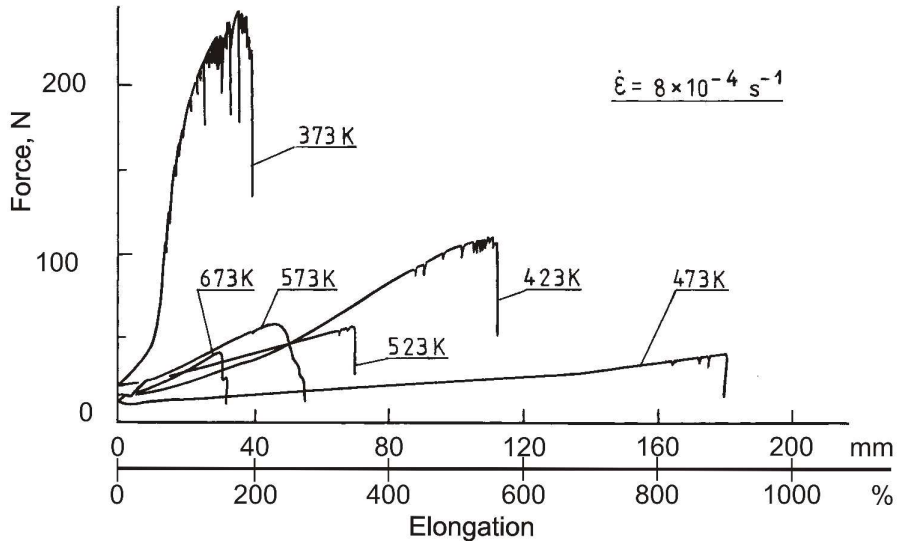

211x144mm (600 x 600 DPI)

View Only

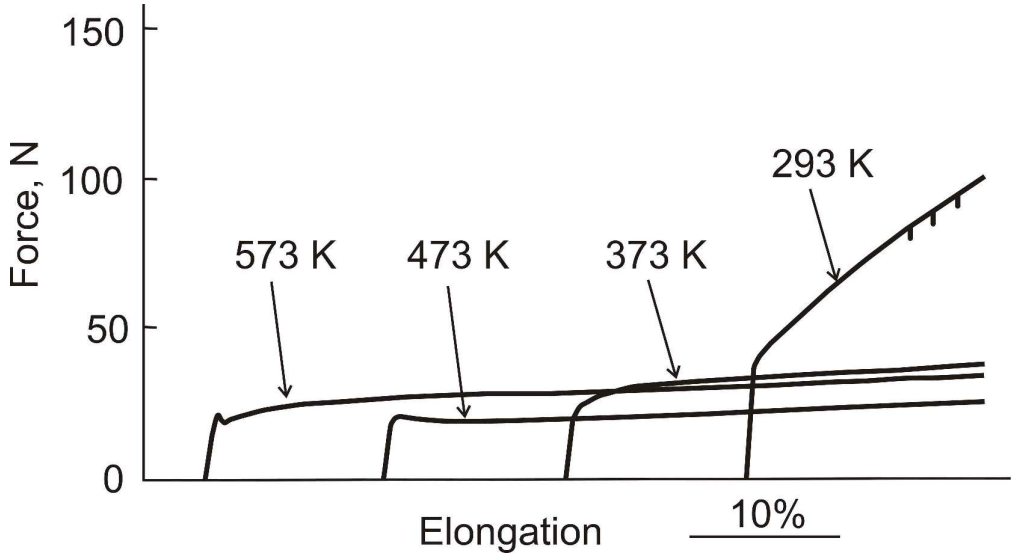

140x77mm (600 x 600 DPI)

Review Only

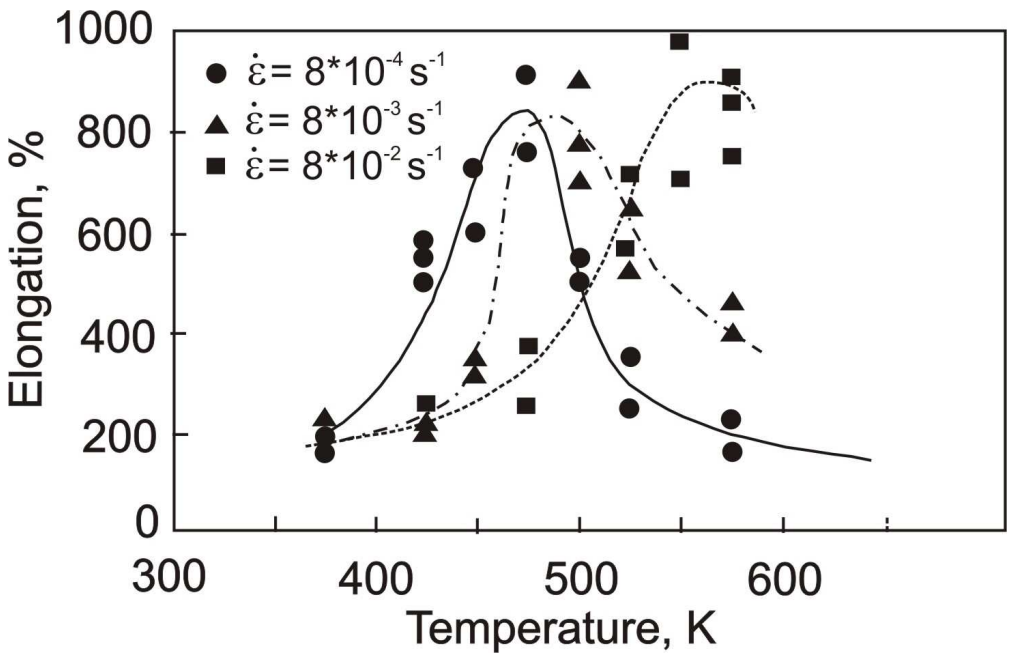

123x79mm (300 x 300 DPI)

For Review Only

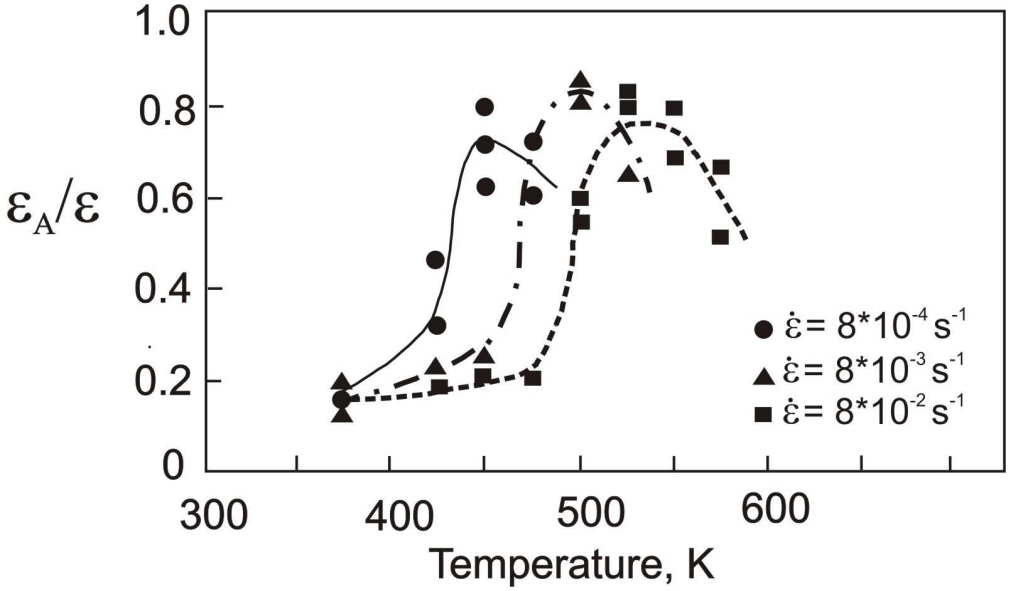

134x78mm (300 x 300 DPI)

Review Only

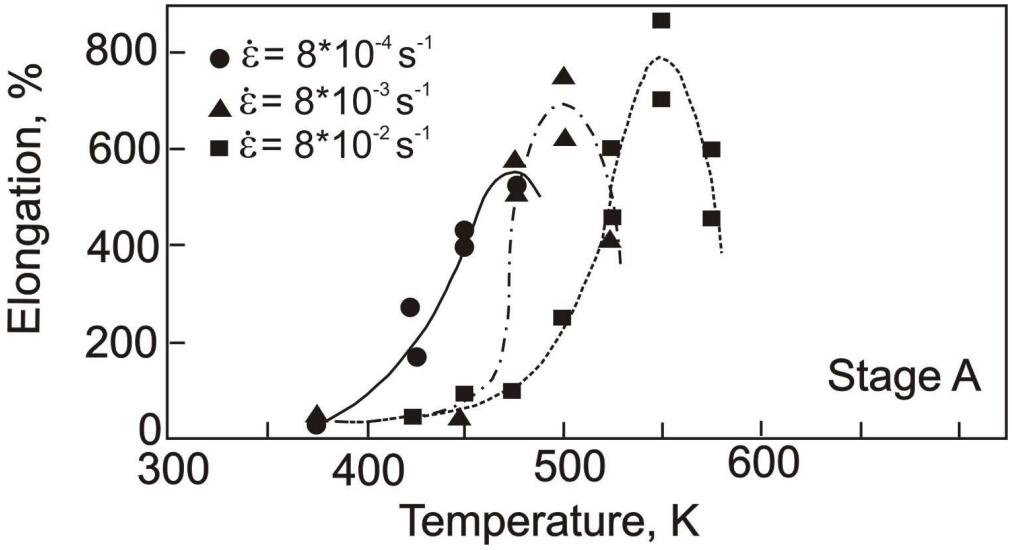

128x69mm (300 x 300 DPI)

Review Only

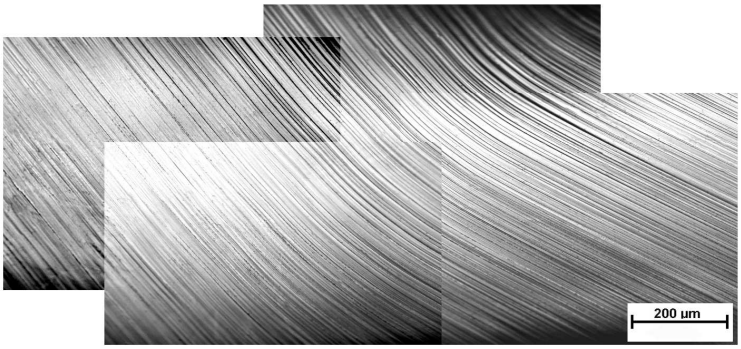

1340x705mm (72 x 72 DPI)

Review Only

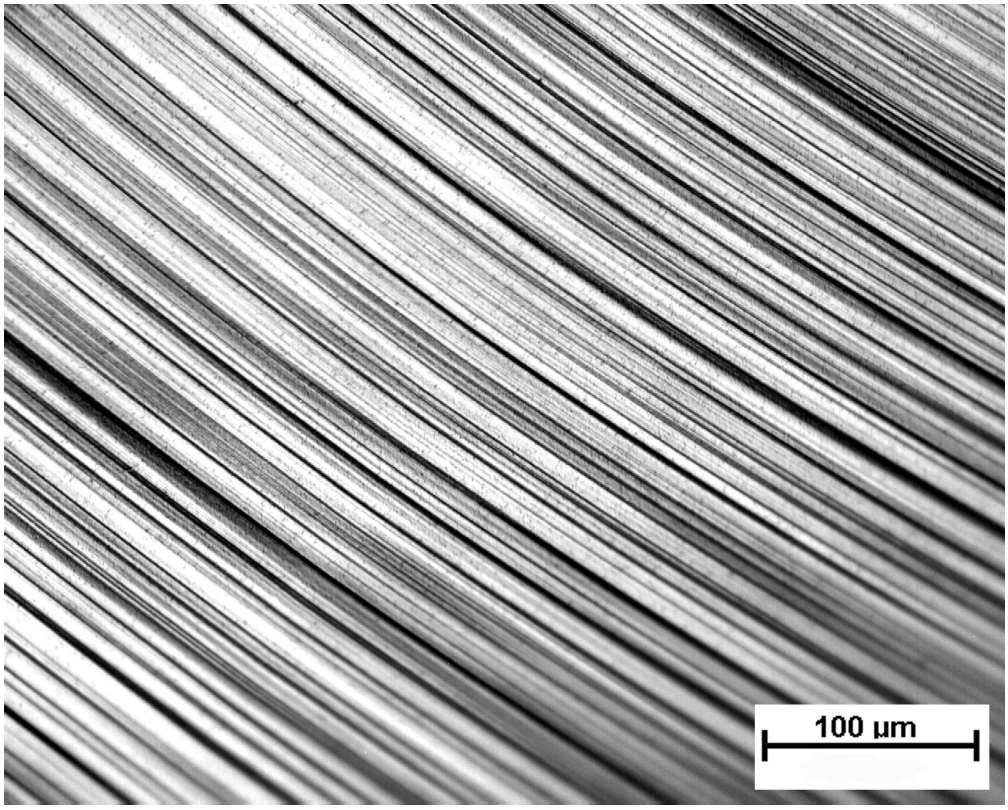

99x80mm (600 x 600 DPI)

w Only

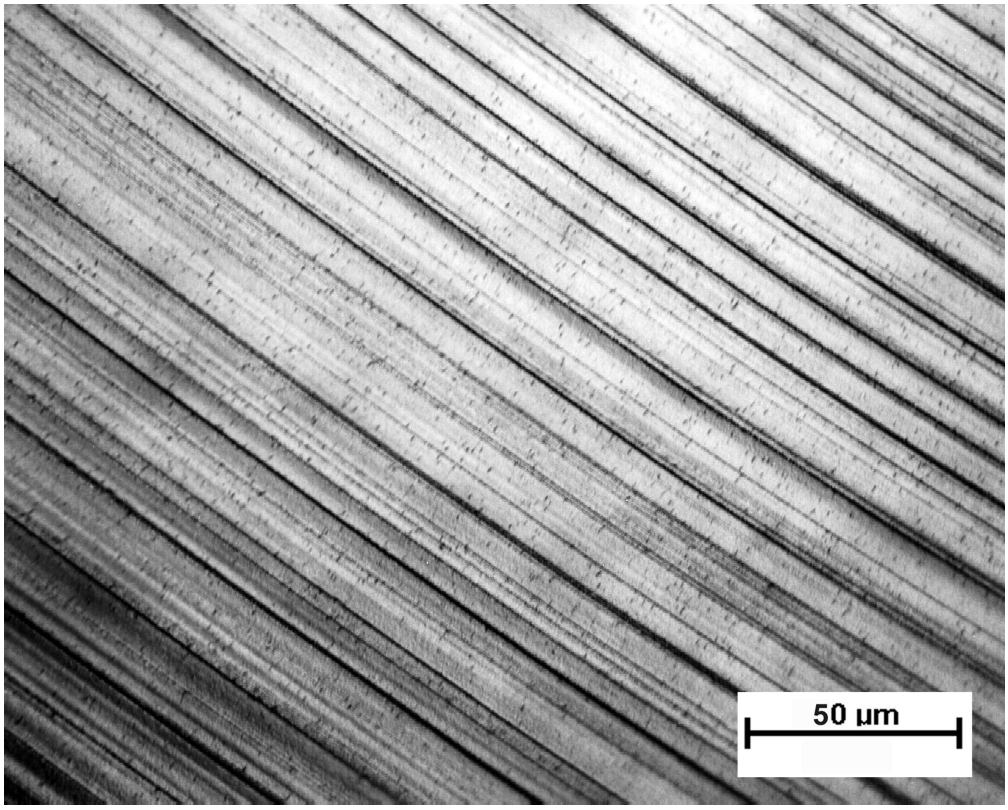

99x80mm (600 x 600 DPI)

w Only

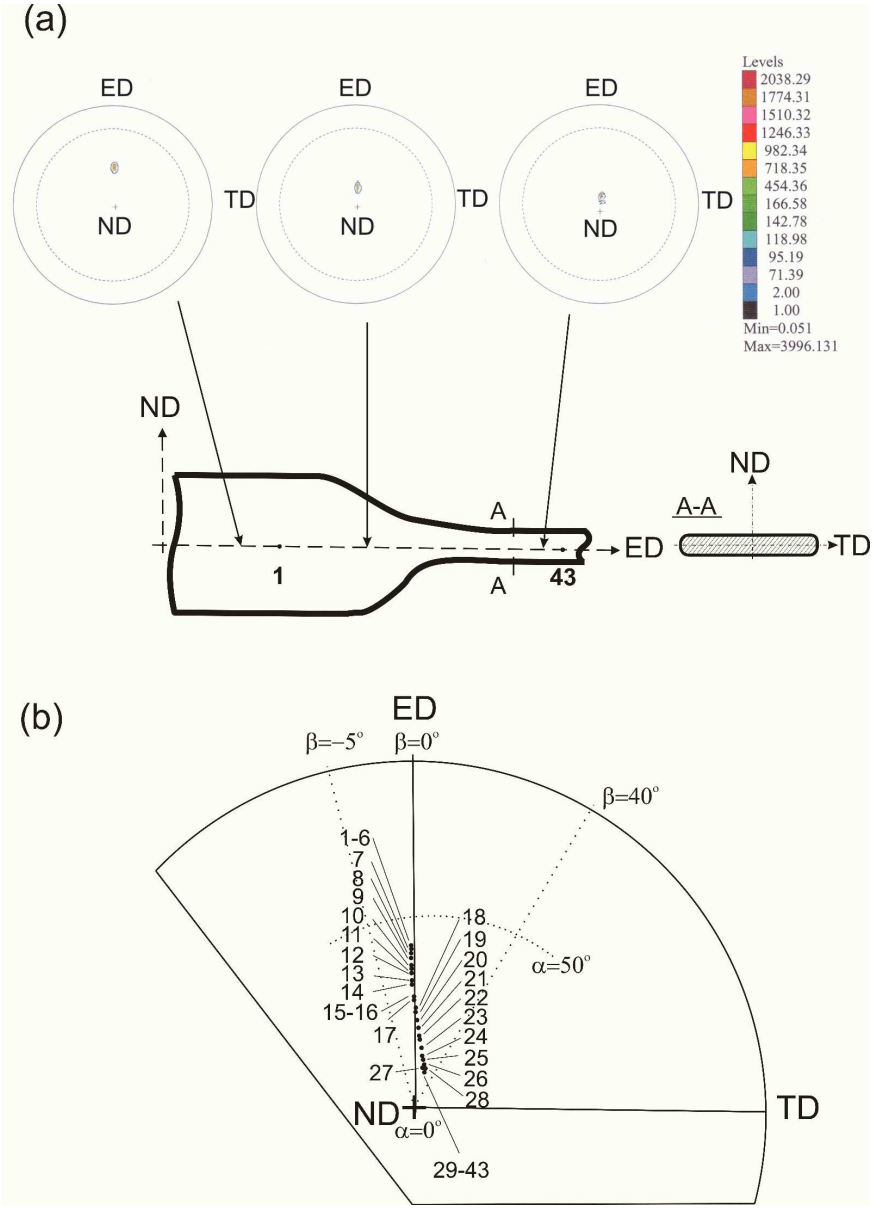

203x280mm (600 x 600 DPI)

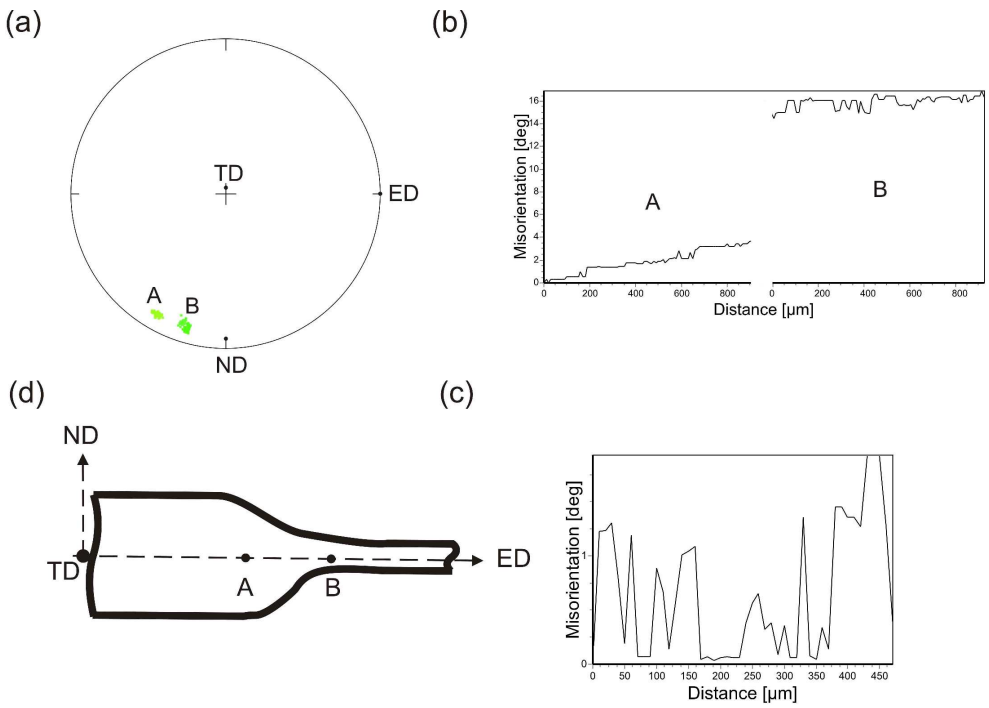

188x132mm (600 x 600 DPI)

View Only

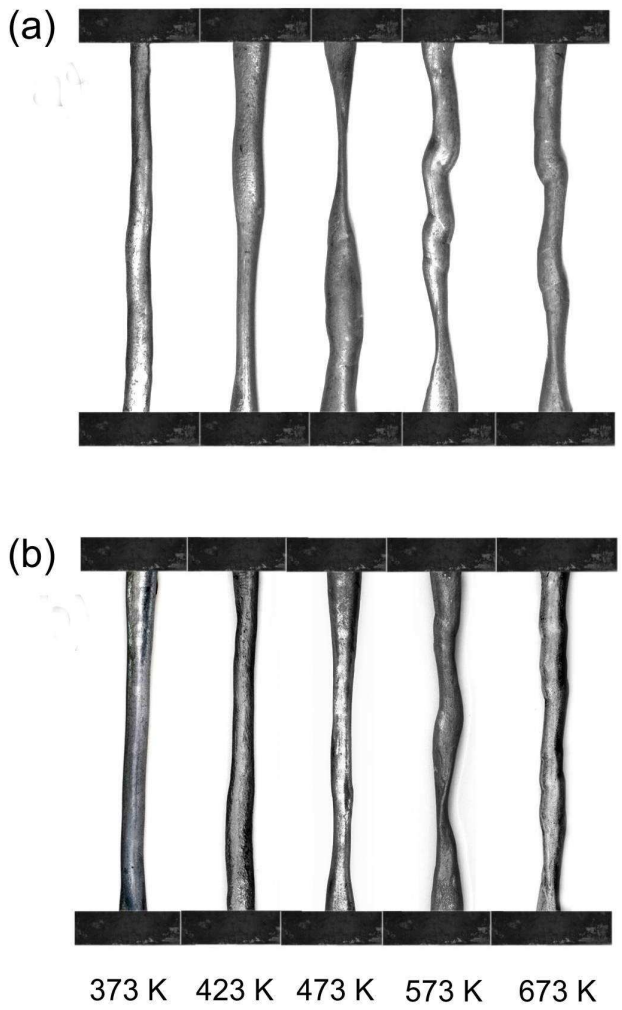

49x84mm (600 x 600 DPI)

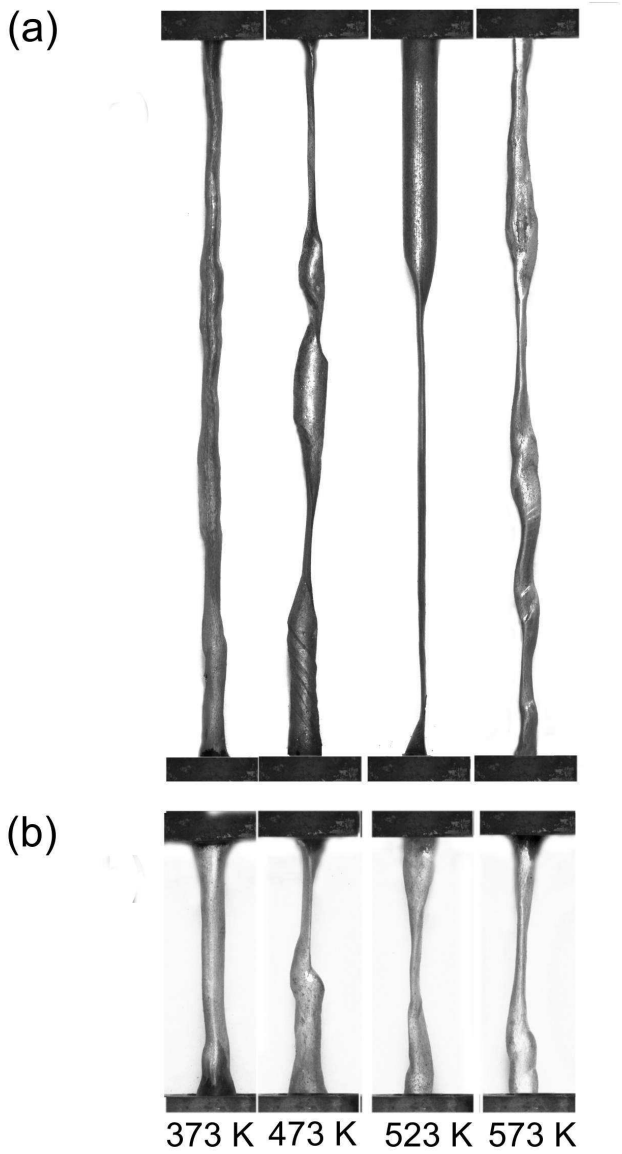

75x99mm (600 x 600 DPI)

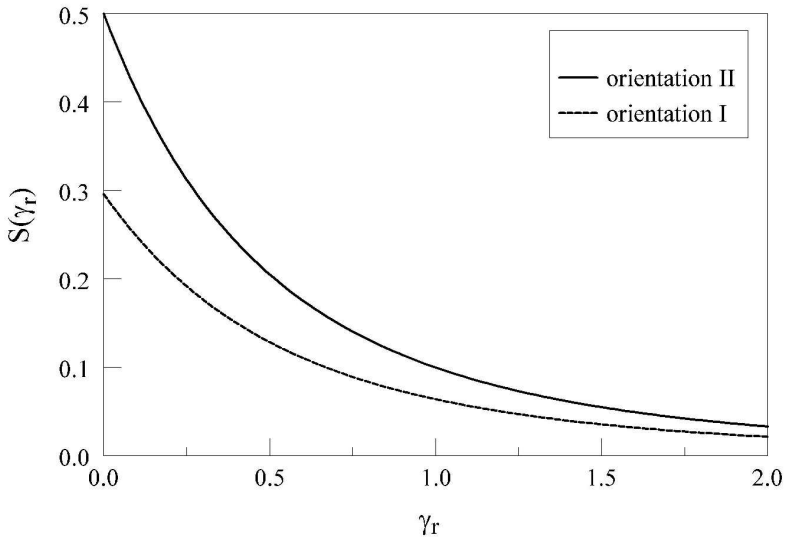

897x672mm (96 x 96 DPI)

For Review Only

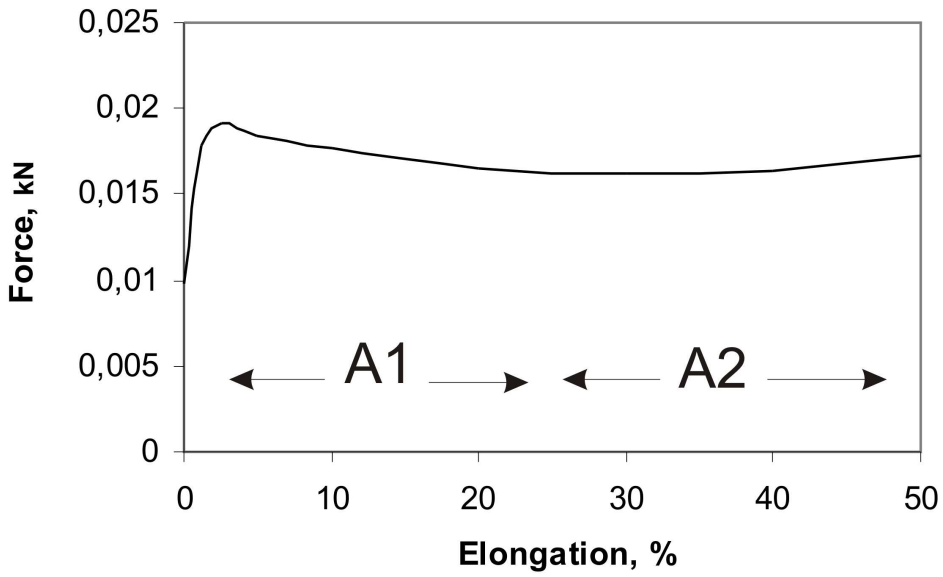

99x66mm (600 x 600 DPI)

View Only

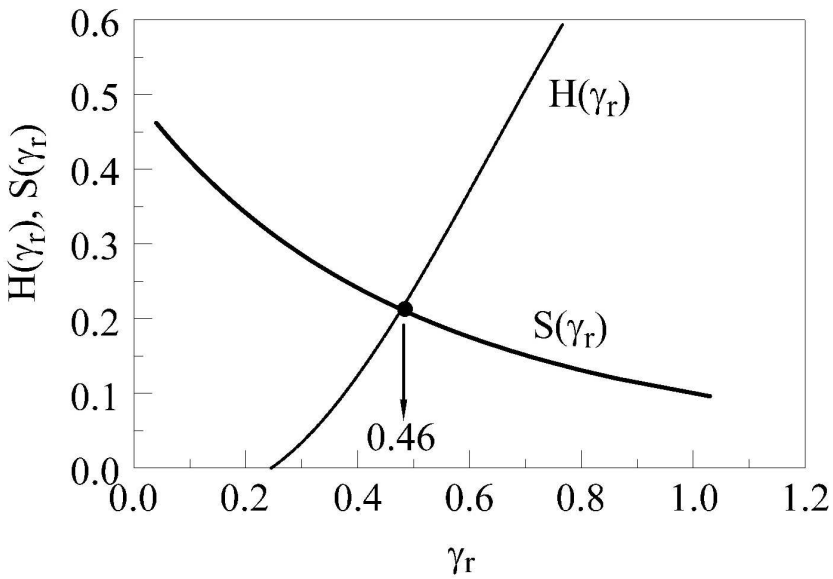

1776x1331mm (96 x 96 DPI)

ew Only

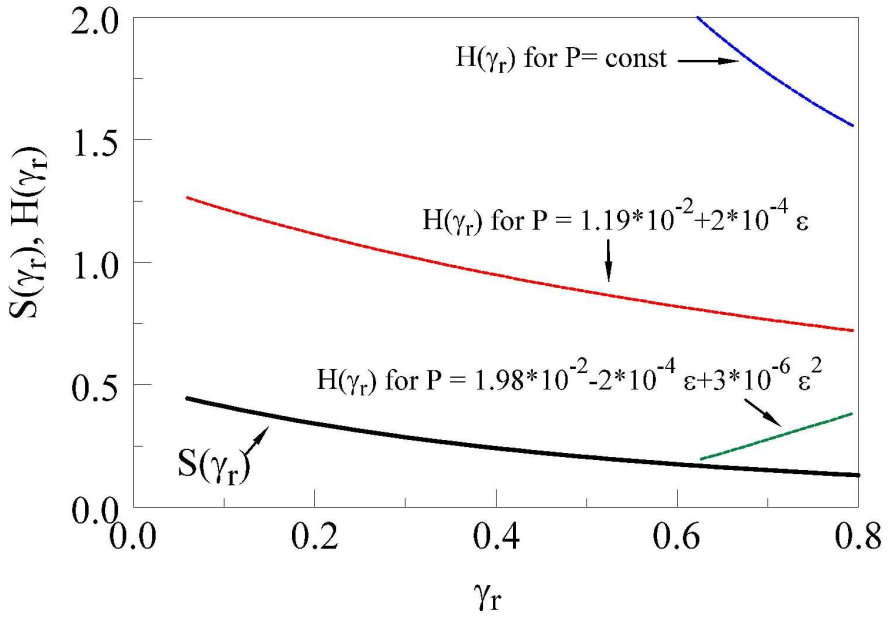

901x674mm (96 x 96 DPI)

ew Only

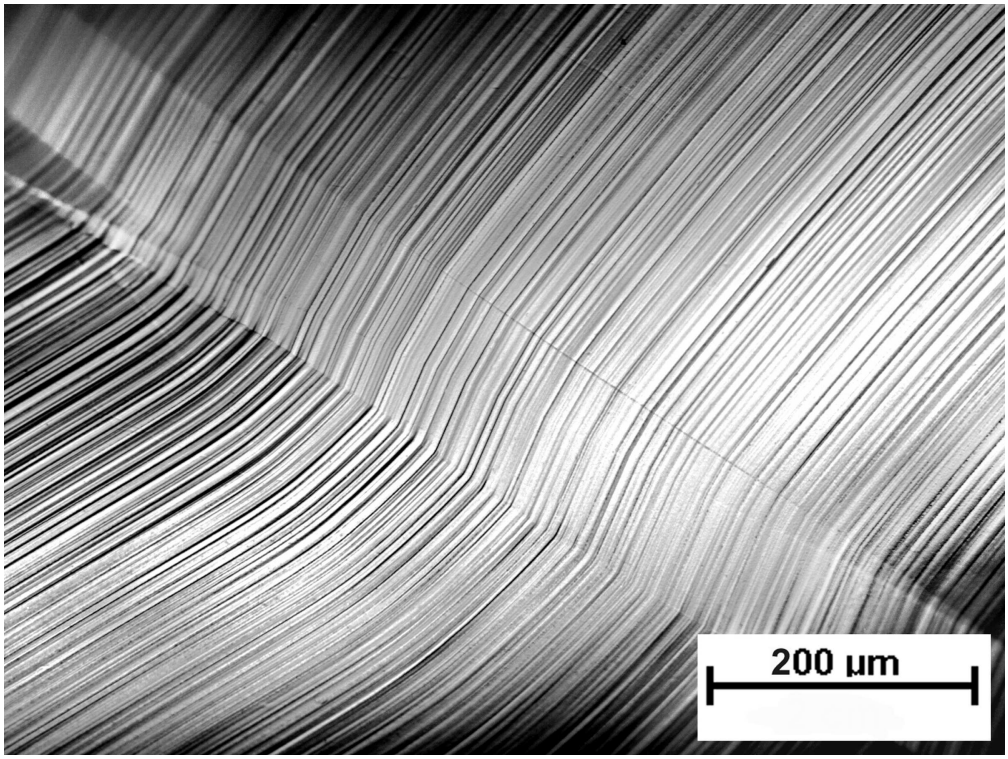

169x127mm (360 x 360 DPI)

ew Only

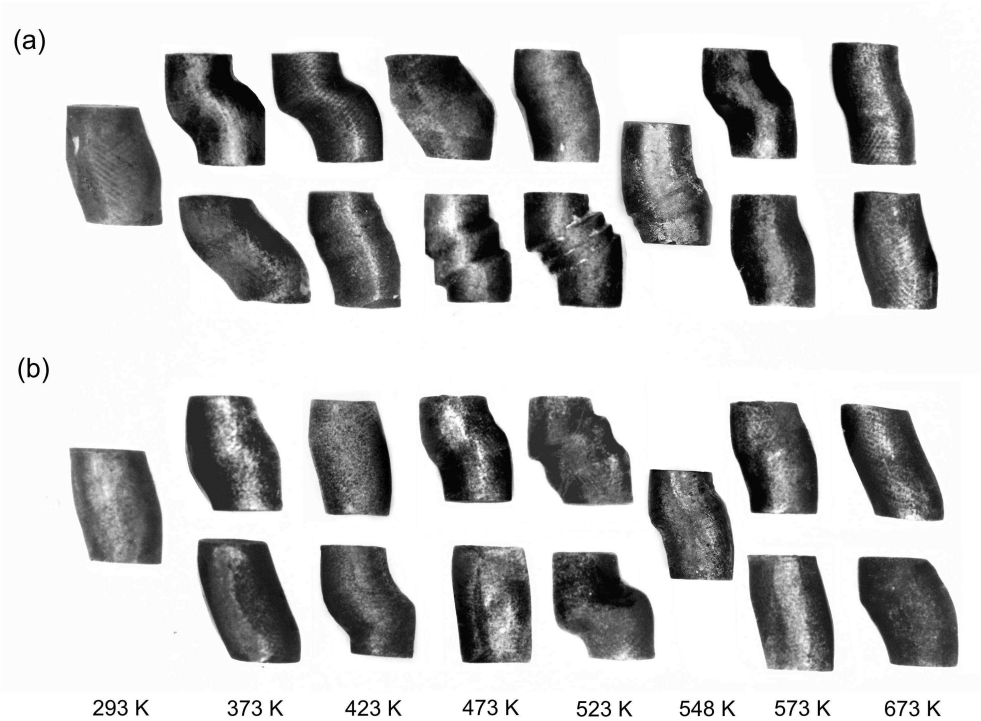

130x96mm (600 x 600 DPI)

ew Only

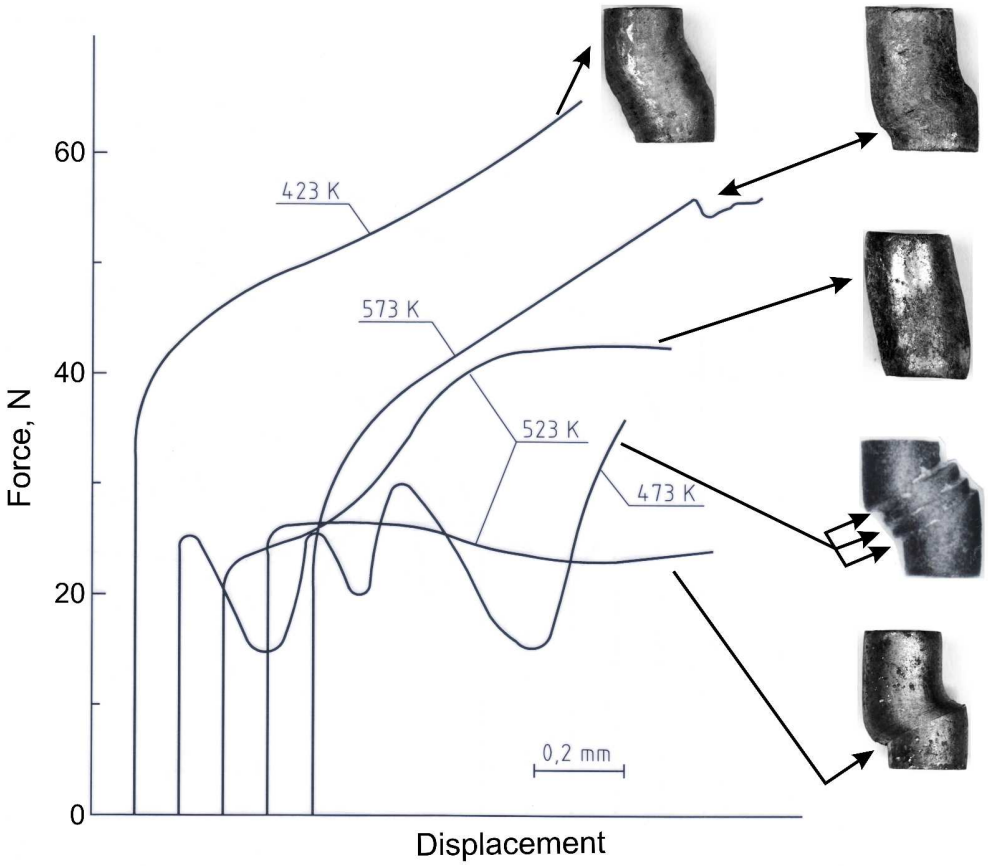

204x180mm (600 x 600 DPI)

Only